Magnetic Skyrmion Dynamics

Felix Büttner
Massachusetts Institute of Technology, Cambridge, Massachusetts
Mathias Kläui
Johannes Gutenberg-Universität Mainz, Mainz, Germany
Graduate School Materials Science in Mainz, Mainz, Germany

In this chapter, the dynamics of magnetic skyrmions is reviewed. Starting with a topological definition of what we call a magnetic skyrmion, we describe the topology and discuss the resulting general properties. To stabilize chiral skyrmions, we introduce a chiral exchange interaction and we present the spin canting that leads to a given handedness for chiral skyrmions. Based on the statics, we next describe the dynamics based on a one-dimensional model and then discuss the steady-state dynamics for instance in wire geometries as well as the gyrotropic relaxation eigenmodes. Finally, we present an experimental demonstration of both these types of dynamics and give a brief outlook on future challenges and opportunities in this field.

8.1 Topological Definition of a Skyrmion

By definition, a vector field is called a skyrmion or said to be skyrmionic if it has a spherical topology. In the following, we will explain the concept of topology, illustrate how the mathematical definition is applied to a magnetic spin configuration, and discuss the implications of a spin structure being a skyrmion.

Topology is a mathematical concept to classify geometrical properties of continuous structures (where structures can be real-space objects, vector fields, momentum space functions, etc.). Two structures are considered equivalent if a continuous map from one to the other exists. There are many possible definitions of continuity inheriting from the large variety of possible complete sets of open subsets of the structure under consideration. Physical constraints, such as energy barriers or forbidden intermediate states, define allowed deformations and the set of prohibited or strongly suppressed transformations. They, therefore, specify meaningful topological distinctions. In physics, topologies are often classified according to homotopic transformations between spaces with Euclidian metric and a Euclidian definition of neighborhood and open sets. A homotopy is a continuous deformation, not necessarily bijective. In contrast, homeomorphisms—defining another possible topological classification—are bijective. For instance, a line and a point are homotopically equivalent, but they are not homeomorph.

To deduce implications of the topology on the physics of a system, the choice of topological classification has to be based on physical arguments. In magnetism, the following three arguments apply. First, in most magnetic systems, the magnetization profile varies on length scales much larger than crystal lattice constants due to the exchange mechanism. Hence, the associated vector field is well described in a continuum model, a prerequisite for a topological classification. Second, exchange interactions, which scale with the gradient of the magnetization, set a natural energy barrier for discontinuous deformations, justifying the concept of homotopy. And third, magnetostatic interactions (anisotropy and stray fields) stabilize the boundary of the structure. Hence, homotopy transformations are allowed, provided that they do not modify the boundary of the structure. This set of allowed transformations (all others are strongly suppressed) defines topological equivalence classes.

One example of a topologically nontrivial structure in real space is the skyrmion. Skyrmions, in general, refer to vector fields with a spherical topology, first identified by T. Skyrme in the field of nuclear physics.[61] Through topological arguments, Skyrme could show the

existence of confined fermionic particle-like solutions of a nonlinear bosonic meson field theory. Specifically, he constructed a field operator that maps the three-dimensional (3D, or 3 + 1 to include the time dimension) domain space to the surface of a sphere.[61] Similarly, the macrospin in micromagnetism is a vector in $\mathbb{R}^3$ with a constant modulus, or, equivalently, a point on the two-dimensional (2D) surface of a sphere S^2. Of particular interest are skyrmionic spin structures in thin films (2 + 1 domain space), i.e., vector fields $\mathbb{R}^2 \to S^2$ that are homotopically equivalent to the identity map on a sphere id_{S^2}. In these structures, the domain space can be continuously deformed to a spherical shape such that the map to the spin space changes continuously, and the boundary of the domain space always maps to the same spin. This homotopy between such so-called magnetic skyrmion and the vector field of a sphere is visualized in Figure 8.1.

The homotopy between a vector field and the identity map on a sphere is described by the topologically invariant skyrmion number N. This counts the number of times the sphere is covered in the homotopical deformation (although if N is not equal to 1, the transformation is much more complicated than illustrated in Figure 8.1 and more difficult to visualize). In two dimensions, the skyrmion number N of a vector field $\mathbb{R}^2 \ni (x, y) \to \mathrm{m} \in S^2$ can be calculated by $N = (8\pi)^{-1} \int \mathrm{d}x\mathrm{d}y n$ with the topological density[2] $n = 2(\partial_x \mathbf{m} \times \partial_y \mathbf{m}) \cdot \mathbf{m}$. Note that the sign in this formula is not consistently defined in the literature, and the definition used here is adapted from Belavin and Polyakov (the first published application of this formula in the field of magnetism that we are aware of).[2]

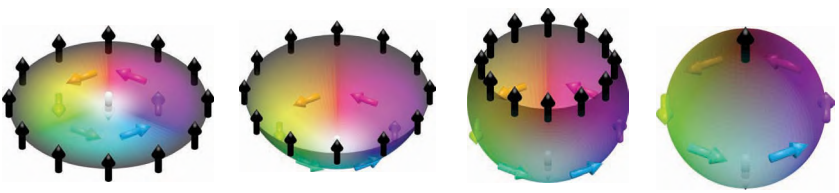

FIGURE 8.1 Homotopy between a skyrmion in a disk and the identity map of the sphere. The hue of the color represents the azimuthal angle of the spins, and the black/white level symbolizes the polar angle. The images show a continuous deformation of the skyrmion (left) to a spherical shape (right). All spins of the skyrmion boundary (black spins) are mapped to the north pole of the sphere, which is only possible because they all point in the same direction. The white spins of the inner domain are all mapped to the south pole. (From Büttner, F., *Topological mass of magnetic skyrmions probed by ultrafast dynamic imaging*. Dissertation, University of Mainz, Mainz, 2013. With permission.)

For our definition and axially symmetric structures (or structures that can be deformed homotopically into axially symmetric shapes) with polarity p and winding number W, the skyrmion number can be calculated by the simplified formula $N = pW/2$.[39] This formula is useful to calculate the skyrmion number "by hand," because the winding number is strictly quantized and it is therefore easy to determine from a picture of the magnetization configuration. The winding number is most conveniently calculated by expressing the 3D macrospin in spherical angles (φ, θ). The winding number of a closed loop is given by the normalized difference of the azimuthal angle φ_i of the spin at an arbitrary point of the loop and the angle φ_f of the spin after going around the full loop once in positive orientation: $W = (\varphi_f - \varphi_i)/(2\pi)$. Naturally, the loop must not cross regions where φ is not well defined (singularities), such as points or areas with pure out-of-plane magnetization or points where two spins are pointing head to head. The winding number is always an integer, and it has nonzero value only if the loop encloses a singularity.[64] Often, only when $W = 1$ (and thus $N = \pm 1$), skyrmionic spin structures are called skyrmions. Note that the magnetization orientation $\mathbf{m}(r,\varphi)$ of circular $W = 1$ skyrmions can be described in polar real-space coordinates (r,φ) by $\mathbf{m}(r,\varphi) = (m_x, m_y, m_z) = (\sin(\theta)\cos(\varphi + \psi), \sin(\theta)\sin(\varphi + \psi), \cos(\theta))$, where $\theta = \theta(r)$ describes the cross-sectional domain wall profile and the constant ψ is the domain wall angle. Skyrmions with $\psi = 0$ (spins pointing outwards) and $\psi = \pi$ (spins pointing inwards) are called Néel skyrmions (sometimes in the literature the term hedgehog skyrmion is also used), whereas skyrmions with $\psi = \pi/2$ (spins rotating counterclockwise) and $\psi = 3\pi/2$ (spins rotating clockwise) are called Bloch skyrmions. The polarity is defined as $p = \frac{1}{2}(m_z(r = 0) - m_z(r = \infty))$.

The skyrmion number provides direct information about the domain structure. The only way to map a planar geometry continuously to a sphere is by contracting its boundary to one single point of the sphere (defining one of the poles). Therefore, all spins on the boundary of an $N = 1$ configuration must have the same orientation, forming a domain. Somewhere in the interior of the configuration, a connected area exists in which the spins point antiparallel to the outer domain (this inner domain can be arbitrarily small down to a single point). The transition between these two domains is a smooth domain wall winding around the inner domain to ensure that the whole sphere is represented. That is, the fact that a spin vector field has $N = 1$ implies the existence of the inner domain, the outer domain, and the domain wall, of which only the outer domain touches the boundary (thus confining the inner

domain and the domain wall). The confined inner domain together with the domain wall has quasiparticle properties, which has led to the name skyrmion.

8.2 General Topological Properties of Skyrmions

The special topology of skyrmions has directly measurable implications; we will discuss four of the key ones here. First, skyrmions are protected against creation or annihilation by a topological energy barrier, as long as they do not move towards the edge of the sample. Due to this topological stability, there is an extended region in the phase diagram where skyrmions and the ferromagnetic state (uniform, parallel spin alignment) have a hysteretic coexistence.[52] In this regime, the number of skyrmions in a given area is a free parameter, which is very important when using skyrmions for data storage technologies. Still, it has been shown that there are ways to create and annihilate skyrmions artificially in this regime of the phase diagram. This can be achieved, for instance, by (1) locally injecting a spin-polarized current,[48,52] (2) locally heating the sample,[31] (3) local magnetic fields,[31] (4) sending a current through a wire with an appropriately shaped constriction,[24,31] (5) high-frequency bipolar excitations in combination with pinning sites,[70] or (6) moving two domain walls[76] or a stripe domain[26] from a constricted area to an extended area. In addition, skyrmions with a finite lifetime, so-called dynamic skyrmions, can be created uniformly in z-direction in a magnetized film by the combined action of the Oersted field and the Slowncewski spin torque of a local current in z-direction that is spin-polarized in z-direction.[75]

A second universal property of magnetic skyrmions is that electrons moving adiabatically across a magnetic skyrmion collect a Berry phase. This phase can be expressed through the Aharonov–Bohm effect caused by an "emergent" magnetic field of the skyrmion. This emergent magnetic field is proportional to the topological density n, and the Berry phase is proportional to the integrated enclosed flux, i.e., to the skyrmion number. The interference of different paths around the skyrmion leads to a deflection of the overall electron propagation direction, i.e., to a transverse current. This leads to a transverse voltage, the so-called topological Hall voltage.[42,53]

A third interesting property of magnetic skyrmions is their outstanding insensitivity to magnetic pinning, at least in the collective motion of densely packed skyrmions, so called skyrmion lattices. One scenario that is particularly interesting for technological applications, such as the racetrack memory proposed by Parkin et al.,[46] is the displacement of

nontrivial magnetic textures by spin-polarized currents. Such nontrivial textures, of which skyrmions are one example, can potentially be used to encode information. The underlying phenomenon for the displacement of spin structures is the so-called spin-transfer torque of conduction electrons on localized spin moments, predicted by Berger[3] and Slonczewski.[62] The investigation of this effect is a subject of intense research nowadays, with a strong focus on the motion of straight domain walls.[5] However, extrinsic magnetic pinning of domain walls has been found to be significant, and mostly no motion has been observed for regular domain walls driven with current densities smaller than 10^{11} A/m^2. In contrast, for skyrmion lattices, this critical current density is five orders of magnitude smaller.[53] So far, no complete theoretical explanation of the particularly low pinning of skyrmions has been published, and it remains to be seen if these low critical current densities can be realized also for isolated skyrmions. However, the confinement of skyrmions intuitively leads to lower pinning compared to extended domain walls. This is firstly because, for topological reasons, skyrmions never touch the edge of the sample, reducing the sensitivity to edge roughness and thus to the main source of pinning. And second, a fully confined structure is flexible to deform and to move around obstacles (provided the obstacles are not attractive).[25,41]

A fourth phenomenon that is directly associated with the skyrmionic topology is a force that acts on a moving skyrmion, pointing perpendicular to its velocity vector. The spherical topology of a skyrmion leads to an intrinsic angular momentum in the quasiparticle equation of motion of a skyrmion,[45] expressed by a gyro term $\mathbf{G}\times\dot{\mathbf{R}}$, where $\mathbf{G} = (0,0,G)$ is the gyrocoupling vector and $\dot{\mathbf{R}}$ is the velocity of the center of mass $\mathbf{R}$ of the skyrmion.[67] The gyrocoupling strength $G = -4\pi NT M_s\gamma$ (where T is the material thickness, M_s its saturation magnetization, and $\gamma = 1.76 \times 10^{11}$ As/kg the gyromagnetic ratio) is proportional to the topological charge N of the skyrmion. Note that the intrinsic angular momentum is zero for skyrmions in antiferromagnets where $M_s = 0$. Intrinsic angular momentum is also found in structures with fractional skyrmion numbers, such as $N = \pm 1/2$ vortices,[23] but generally not in straight domain walls with $N = 0$.

8.3 Chiral Exchange Interactions

The spin structures present in a system generally result from the minimization of the relevant micromagnetic energy terms. In addition to the Heisenberg exchange that favors spin structures with random chirality, chiral skyrmions can be stabilized by chiral exchange interactions that can be found in systems with inversion asymmetry and strong spin–orbit

coupling (SOC). The so-called Dzyaloshinskii–Moriya interaction (DMI) is a symmetry-breaking (antisymmetric) exchange interaction that is present in addition to the Heisenberg exchange. The DMI between two spins in a magnetic material is mediated via the SOC of an adjacent heavy-metal atom with strong spin–orbit interaction, as shown schematically in Figure 8.2. Taking into account SOC, Moriya found that the effective Hamiltonian for the interaction between two (macro-)spins $\mathbf{M}_1$ and $\mathbf{M}_2$ contains a term $\mathbf{D}_{12} \cdot (\mathbf{M}_1 \times \mathbf{M}_2)$.[38] As shown schematically in Figure 8.2, a DMI coupling can arise at the interface of a heavy metal layer and a ferromagnetic layer (FL) in a multilayer stack due to the broken inversion symmetry in z-direction and the strong SOC of the heavy metal. The resulting DMI vector, $\mathbf{D}_{12}$, points in the plane of the layers and perpendicular to the vector connecting $\mathbf{M}_1$ and $\mathbf{M}_2$. The magnitude and the sign of $\mathbf{D}_{12}$ are properties of the interface and the involved materials. The DMI leads to a favored chirality of a spin spiral state.[12,51] For sufficiently strong DMI, a spin spiral state is favored with the spiral axis in the plane.[47] For lower values of D, a skyrmion lattice is the ground state.[40] While DMI is not necessary to obtain skyrmion spin structures with a given topology as they can be stabilized by dipolar interactions for instance in thin films, the DMI modifies the spin structure.[30] In general, in thin film multilayers, both dipolar interactions and DMI will be present as it has been shown that even for nominally symmetric stacks, DMI is present due to the different growth at the interfaces.[20]

Overall, strong DMI will increase the stability of spin structures and favor skyrmions with a certain topology ($W = 1$ winding number) and a fixed product ψp of domain wall angle ψ and polarity p, which, however, is not a topological quantity in a homotopic classification.

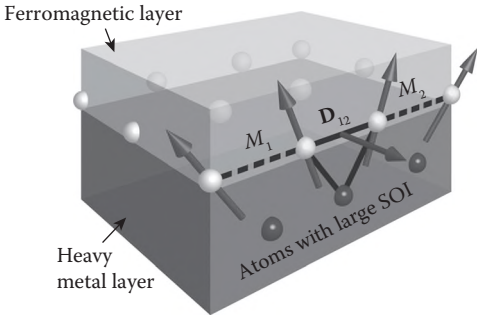

FIGURE 8.2 Illustration of the Dzyaloshinskii–Moriya interaction. In multilayer stacks with broken inversion symmetry, chiral coupling between two spins M_1 and M_2 is mediated by a heavy atom (dark gray) in one of the nonmagnetic layers (HL). The sign and strength of the resulting DMI (vector $\mathbf{D}_{12}$) are interface/materials' properties that lead to one favored chirality of the spin structure.

8.4 Quasiparticle Equation of Motion

Here, we present the general quasiparticle equation of motion of a $W = 1$ rigid circular skyrmion, including the effects of spin-polarized electrical currents and uniform spin injection due to the spin Hall effect (SHE) in an adjacent heavy metal layer. An electrical current flowing through a ferromagnetic material gets polarized along the local magnetization direction. The spin-polarized current is parametrized by the spin drift velocity $\mathbf{u} = \mathbf{J}P\mu_B/(eM_s)$, where $\mathbf{J}$ is the electron current density, P is the spin polarization of the material, $\mu_B = 9.27 \times 10^{-24}$ J/T is the Bohr magneton, and $e = 1.602 \times 10^{-19}$ C is the electron charge. At a gradient of the magnetization, the re-orientation of the conduction electron spins requires the transfer of angular momentum to the local magnetization. This transfer of angular momentum can be due to adiabatic or nonadiabatic spin-transfer torques, but the torque on the local magnetization is always proportional to the gradient of the magnetization and as such it is a function of position in the sample. In contrast, a heavy metal layer above or below the ferromagnetic layer becomes a source of a uniform (position-independent) spin current when it is transmitted by an electrical current $\mathbf{j}_{HM}$. The spin current flows perpendicular to $\mathbf{j}_{HM}$ and is polarized perpendicular to both $\mathbf{j}_{HM}$ and to the spin current direction. The injection of angular momentum leads to a torque on the magnetization, which can be described by a sum of the two terms: a contribution that acts like a uniform magnetic field along the polarization of the injected spins (field-like term) and one term that resembles the damping term of the Landau–Lifshitz–Gilbert equation (damping-like term). Here, we only consider the damping-like term because a uniform field does not cause motion if we assume the skyrmion to be rigid. Taking into account all these contributions, the resulting quasiparticle equation of motion for the center of mass position $\mathbf{R}$ reads[17,24,34,52,66,68]:

$$-M\ddot{\mathbf{R}} + \mathbf{G}\times(\dot{\mathbf{R}} - \mathbf{u}) - \tilde{D}(\alpha\dot{\mathbf{R}} - \beta\mathbf{u}) + 4\pi B\tilde{R}(\psi)\mathbf{j}_{HM} + \mathbf{F} = 0, \tag{8.1}$$

where M is the effective mass of the skyrmion, $\tilde{D} = TM_s\gamma\int \mathrm{d}x\mathrm{d}y\left(\partial_x \mathbf{m}\right)^2$ is the dissipation constant, α is the Gilbert damping, β is the nonadiabaticity parameter, $B = \dfrac{\gamma^2\hbar\theta_{SH}}{2e}I$ is a coefficient that depends on the spin configuration (with the reduced Planck constant $\hbar = 6.63 \times 10^{-34}$ Js, the spin Hall angle θ_{SH}, and $I = \dfrac{1}{4}\int_0^\infty \mathrm{d}r\left(\sin\theta\cos\theta + r\dfrac{\mathrm{d}\theta}{\mathrm{d}r}\right)$)

$\tilde{R}(\psi) = \begin{pmatrix} \cos\psi & \sin\psi \\ -\sin\psi & \cos\psi \end{pmatrix}$ is the rotation matrix corresponding to the domain wall angle ψ, $\mathbf{j}_{HM}$ is the current density of an adjacent spin Hall heavy metal, and $\mathbf{F}$ is a driving force acting on the skyrmion for instance due to a gradient of the out-of-plane effective field. The center of mass of a skyrmion is determined from an average position of its spins (the spins enclosed by the loop of spins with zero out-of-plane moment) weighted by their out-of-plane component. Note that Equation 8.1 is written in a form that each term is given in units of force. Sometimes, another form is found in the literature, where the whole equation is divided by $TM_s\gamma$, thus giving each term the units of velocity.[24,52,68] In that form, the gyrocoupling constant and the dissipation constant reduce to $G' = -4\pi N$ (or sometimes $G' = 4\pi N$) and $\tilde{D}' = \int \mathrm{d}x\mathrm{d}y(\partial_x \mathbf{m})^2$, respectively.

The overall dynamics of skyrmions are well described by Equation 8.1. However, some details of the trajectories that are visible in micromagnetic simulations cannot be explained by this equation. Therefore, a number of modifications to Equation 8.1 were suggested. These include adding a gyrodamping[55] and making the parameters of the equation dependent on the excitation type (thermal, spin current, or field gradient) and the excitation frequency.[55] Yet, the magnitude and significance of such corrections still have to be determined from experiments. The few existing experiments are described well by Equation 8.1, and we therefore discuss the dynamics of skyrmions based on this equation in the following section.

8.5 Dynamics of Skyrmions

In this section, we discuss the dynamics of magnetic skyrmions in three distinct scenarios: (1) the steady-state motion, which skyrmions will enter if the excitation is constant or varies only very slowly, (2) the gyrotropic eigenmodes in a parabolic potential, and (3) the translational motion along a nanowire using pulsed forces.

8.5.1 Steady-State Motion

Due to the gyro term in Equation 8.1, the x and y position coordinates, R_x and R_y, are canonically conjugate variables,[25] similar to position and transverse spin angle for straight domain walls[36] (the transverse

spin angle is the angle of the spins with respect to the plane formed by the set of all spins in the domains and in the domain wall at rest). Therefore, in the absence of confining potentials (and pinning, i.e., $\mathbf{F} = 0$), the steady-state motion of a skyrmion is a linear trajectory with a characteristic angle with respect to the direction of the driving force, the skyrmion Hall angle. The velocity depends linearly on the excitation strength, i.e., there is no intrinsic pinning, which is in stark contrast to the dynamics of nontopological domain walls. The steady-state velocity for a spin current in x-direction ($\mathbf{u} = (u,0,0)$) is given by[25]:

$$\dot{R}_x = \left(\frac{\beta}{\alpha} + \frac{\alpha - \beta}{\alpha^3 (\tilde{D}/G)^2 + \alpha} \right) u, \tag{8.2}$$

$$\dot{R}_y = \frac{(\alpha - \beta)(\tilde{D}/G)}{\alpha^2 (\tilde{D}/G)^2 + 1} u. \tag{8.3}$$

Often, $\alpha \ll 1$ and $\tilde{D}/G \leq 1$, which means that Equations 8.2 and 8.3 can be simplified to[25]:

$$\dot{R}_x \approx u, \tag{8.4}$$

$$\dot{R}_y \approx (\alpha - \beta)(\tilde{D}/G) u. \tag{8.5}$$

Hence, within this approximation, the velocity in the direction of the current flow $\dot{R}_x$ does not depend on α or β; only the skyrmion Hall angle $\tan(\xi) = \dot{R}_y / \dot{R}_x$ is influenced by these material parameters. Remarkably, the skyrmion Hall angle for current-driven skyrmion motion scales inversely with the topological charge N (remember $G \propto N$), whereas in cases of skyrmion motion driven by a finite force $F_x \neq 0$ (as, for instance, due to a magnetic field gradient), the spin Hall angle scales linearly with N[36]:

$$\tan(\xi) = -\frac{2N\Delta_0}{R\alpha}, \tag{8.6}$$

where Δ_0 is the domain wall width parameter of the skyrmion domain wall and R is the skyrmion radius.

If the skyrmion is driven by a constant spin injection due to a spin Hall current $\mathbf{j}_{HM} = (j_{HM},0,0)$ instead of a spin current u, then the steady-state velocity depends on the chirality of the skyrmion. Essentially, the skyrmion is dragged in the direction where the spins in its domain

wall are parallel to the injected spins.[68] The steady-state velocity for an $|N| = 1$ skyrmion in this case reads:

$$\dot{R}_x = \left[\frac{\alpha \tilde{D} B}{G^2 + \alpha^2 \tilde{D}^2} \cos(\psi) + \frac{GB}{G^2 + \alpha^2 \tilde{D}^2} \sin(\psi) \right] j_{\mathrm{HM}}, \tag{8.7}$$

$$\dot{R}_y = \left[-\frac{\alpha \tilde{D} B}{G^2 + \alpha^2 \tilde{D}^2} \sin(\psi) + \frac{GB}{G^2 + \alpha^2 \tilde{D}^2} \cos(\psi) \right] j_{\mathrm{HM}}, \tag{8.8}$$

indicating that a Néel skyrmion with low damping $\alpha \ll 1$ moves perpendicular to the spin Hall current, whereas a Bloch skyrmion moves in the direction of the injected spin Hall current.[68]

In case of a confining potential in *y*-direction and a spin current in *x*-direction (as experienced by a skyrmion in a nanowire), the current-driven skyrmion dynamics change drastically. Here, the skyrmion first moves on a diagonal line towards higher potential energy regions (towards the edge of the wire) before entering a steady-state longitudinal motion. The angle between the diagonal line of the initial motion and the *x*-axis is again the skyrmion Hall angle, and the velocity of the subsequent longitudinal motion of the skyrmion follows the same equations as that of a straight domain wall.[24]

8.5.2 Gyrotropic Eigenmodes

The dynamics of skyrmions is particularly rich in the case of non-steady-state motion, for instance due to pulsed spin currents or due to pinning ($\mathbf{F} \neq 0$). In those cases, inertia of the skyrmion becomes important. The simplest case is the motion of a skyrmion in a radially symmetric parabolic potential in the absence of currents or field gradients, i.e., for $\mathbf{F} = -K\mathbf{R}$ and $\mathbf{u} = 0$. Here, K is the potential stiffness. In reality, most potentials can be locally approximated by a parabola, which makes this analytically solvable approximation applicable to experimental situations. Therefore, we will discuss the solution of the equation of motion for this particular case in more detail.

As a reminder, the equation of motion for a skyrmion in a parabolic potential without current reads:

$$-M\ddot{\mathbf{R}} + \mathbf{G} \times \dot{\mathbf{R}} + \tilde{D}\alpha\dot{\mathbf{R}} - K\mathbf{R} = 0. \tag{8.9}$$

By using the convenient complex parametrization $\overline{R} = R_x + iR_y$ of the location vector, we obtain:

$$-M\ddot{\overline{R}} + (\tilde{D}\alpha + iG)\dot{\overline{R}} - K\overline{R} = 0, \tag{8.10}$$

which is a simple harmonic oscillator with solution:

$$\bar{R}(t) = A\exp(i\bar{\omega}_1 t) + B\exp(i\bar{\omega}_2 t) \tag{8.11}$$

with:

$$\bar{\omega}_{1,2} = i\eta \pm \sqrt{\omega_0^2 - \eta^2}\,, \tag{8.12}$$

$$\eta = -\frac{1}{2M}(\tilde{D}\alpha + iG), \tag{8.13}$$

$$\omega_0 = \sqrt{K/M}\,. \tag{8.14}$$

The two terms of the sum in Equation 8.11 are called gyrotropic eigenmodes of the skyrmion. They describe a left-handed and a right-handed spiraling motion, respectively. The complex frequencies $\bar{\omega}_{1,2} = \omega_{1,2} + i/\tau_{1,2}$ combine the real frequencies of the spiraling motion $\omega_{1,2}$ and the damping $\tau_{1,2}$ in one number. When both modes are excited simultaneously, the resulting trajectories can have distinctly different shapes depending on the relative amplitude of the modes, see Figure 8.3. If the lower frequency mode has a smaller amplitude than the higher frequency mode, the trajectory looks like a deformed spiral, which rotates clockwise if N is positive, and counterclockwise if N is negative

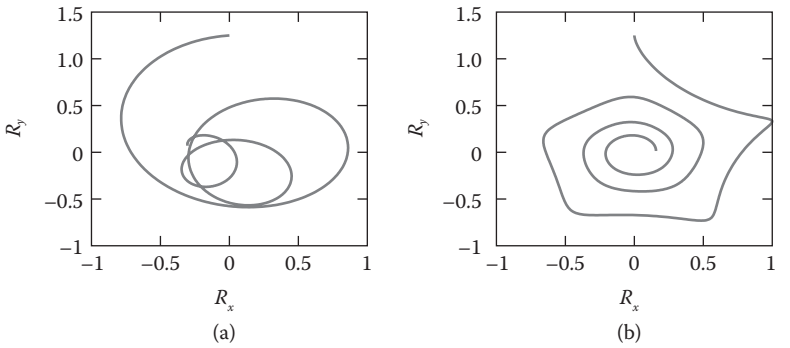

FIGURE 8.3 Micromagnetically computed trajectories of a skyrmion in a parabolic potential. In both graphs, $\omega_1/\omega_2 = -4$ and N is negative. (a) The amplitude of the higher frequency mode ω_1 is initially four times larger than that of the lower frequency mode ω_2. The trajectory is a deformed spiral rotating counterclockwise. (b) The amplitude of the higher frequency mode is initially four times smaller than that of the lower frequency mode. The trajectory is a hypocycloid with $5 = -\omega_1/\omega_2 + 1$ cusps per turn, rotating clockwise.

(Figure 8.3a). If the lower frequency mode has a larger amplitude than the higher frequency mode; however, the trajectory becomes a hypocycloid and the rotation is reversed (counterclockwise if N is positive and clockwise if N is negative). The number of cusps is given then by $-\omega_1/\omega_2 + 1$ (Figure 8.3b). Note that the damping scales linearly with the frequency.[34] Therefore, a trajectory as in Figure 8.3a will at a later time transform into a motion that resembles Figure 8.3b (and thereby changing the sense of rotation). Even later, the amplitude of the lower frequency mode will be so small that the trajectory cannot be distinguished from that of a massless skyrmion within the experimental resolution.

Only $|N| = 1$ skyrmions show the previously discussed gyrotropic eigenmodes. Skyrmions of other topological charges show complex dynamics within their domain wall during the motion, which means that the spin structure no longer behaves like a rigid particle. Hence, Equation 8.1 is no longer able to describe the dynamics of the skyrmion as a whole on the time scale of the domain wall fluctuations.

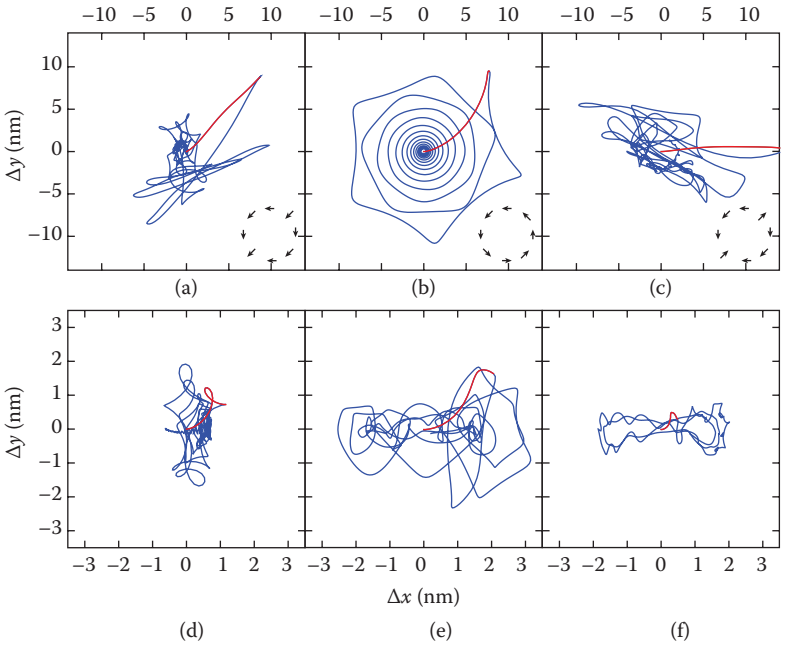

FIGURE 8.4 Trajectories of variable N skyrmions in a parabolic potential: (a) $N = 0$, (b) $N = 1$, (c) $N = 2$, (d) $N = 3$, (e) $N = 4$, and (f) $N = 5$. The red lines indicate the trajectory during the excitation with a magnetic field gradient. The blue lines indicate the relaxational motion. The insets in (a–c) schematically show the spin structures of the domain walls of an $N = 0$, $N = 1$, and $N = 2$ skyrmion, respectively. (From Felix, B, *Nat. Phys.*, 11, 225–228, 2015. With permission.)

The resulting trajectories are visualized in Figure 8.4 for $N = 0,1, ..., 5$. For the dynamics on timescales much slower than the domain wall fluctuations, however, Equation 8.1 has been found to be very accurate even up to $N = 90$.[36]

The eigenfrequencies $\omega_{1,2}$ and the corresponding damping terms $\tau_{1,2}$ can be measured in an experiment, for instance by resonant excitations[43,57] or by imaging the trajectory.[11] Figure 8.5 shows the 2D relaxational trajectory of a skyrmion after displacement in a parabolic potential, measured with 3 nm spatial precision and 50 ps temporal resolution.

The experimental skyrmion trajectory in Figure 8.5 is in excellent agreement with the theoretical prediction of Equation 8.11 if both gyrotropic eigenmodes are considered. The existence of two gyrotropic eigenmodes is an unambiguous indicator for an $|N| = 1$ spin structure topology. Furthermore, the frequencies can be used to calculate the mass of the skyrmion:

$$\omega_1 + \omega_2 = \mathrm{Re}(\bar{\omega}_1 + \bar{\omega}_2) \tag{8.15}$$

$$= \mathrm{Re}(G/M - iD\alpha M) \tag{8.16}$$

$$= G/M. \tag{8.17}$$

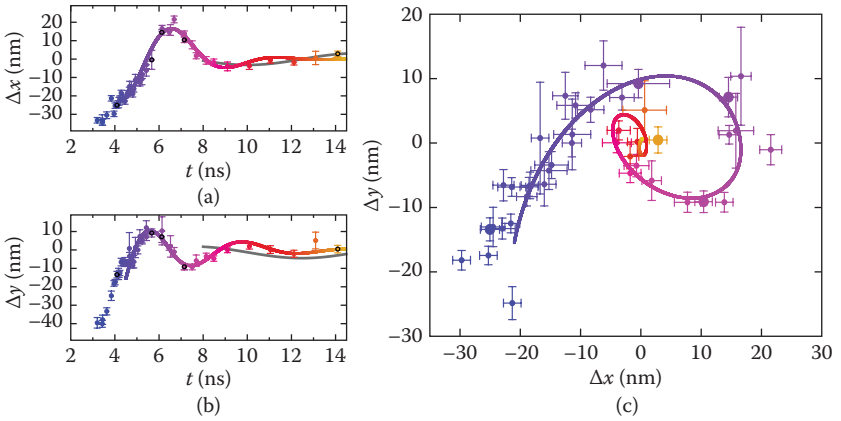

FIGURE 8.5 Gyrotropic trajectory of an $N = 1$ skyrmion, with (a) and (b) showing the temporal evolution of the x and y coordinate of the skyrmion, respectively, and (c) depicting the x-y trajectory. Data points plot positional changes of the skyrmion extracted from dynamic imaging of its relaxational motion after excitation in a parabolic potential. Colored lines represent a fit of the data points with the theoretical model of Equation 8.11. Gray lines depict the best fit with Equation 8.11 when setting the mass to zero. (From Büttner, F. *Nat. Phys.*, 11, 225–228, 2015. With permission.)

In the experiment, the frequencies were of the order of 1 GHz. The corresponding mass of the skyrmion has been found to exceed the inertia of its domain wall, the so-called Döring mass,[14] by at least a factor of 5.[11] In brief, the Döring mass of a domain wall originates from the fact that a domain wall can only move if its spins tilt out of their equilibrium position, which increases the magnetostatic energy. The increase in energy by tilting the spins is described by an effective anisotropy[9] $K_\perp$ and the Döring mass of a domain wall of width Δ_0 reads:

$$m_D = \frac{M_s^2(1+\alpha^2)}{K_\perp \gamma^2 \Delta_0}, \tag{8.18}$$

where $\gamma = 1.76 \times 10^{11}$ As/kg is the gyromagnetic ratio. Skyrmions, however, posses a mass that is significantly larger than expected from the domain wall theory, thus indicating further contributions to their inertia. It was suggested that the expansion and shrinking of the skyrmion, the so-called breathing mode, constitutes another source of inertia as this mode can store energy.[54] This source of inertia is only found in skyrmionic spin structures because the skyrmions are the only completely confined spin structures in magnetism, i.e., the only structures that can continuously grow and shrink. The large mass of the skyrmion has hence been called topological mass.[11]

8.5.3 Motion along Nanowires

The dynamics of skyrmions in fully confining potentials as discussed before is best suited for studying their quasiparticle properties as well as for applications in radio-frequency technology, where the skyrmions are excited at their resonance frequency.[57] Most other possible applications, however, rely on skyrmions being displaced to a new equilibrium position. In this complicated scenario, Equation 8.1 has to be solved numerically. Research in this field has just started and a more complete picture is still emerging. Here, we first demonstrate that inertia of a skyrmion does not impact how far the skyrmion is displaced but that the trajectory of the motion in between depends on the magnitude of the mass. Subsequently, we discuss the first experimental observation of the propagation of skyrmions.

A typical potential application of propagating skyrmions is in a magnetic shift register.[18] In this application, skyrmions are placed in a nanowire. A pulsed current or a pulsed magnetic field gradient are applied in the direction of the wire in order to move the skyrmions by a well-defined distance. Ideally, there is no other force along the

direction of the wire (i.e., no pinning), and the potential perpendicular to the wire can be approximated by a parabola. The trajectories of a massive and a massless skyrmion in such an ideal scenario for the case of a pulsed force (and without current) are compared in Figure 8.6. The mass of the massive skyrmion, $M = 2 \times 10^{-21}$ kg, is the mass found in the experiment in Ref. [11]. Both skyrmions, the massive and the massless, travel the exact same distance. The massive skyrmion, however, needs more time to arrive at the new equilibrium position, and the transverse displacement during the motion is significantly smaller than for the massless skyrmion. Hence, a massless skyrmion is more likely to be annihilated when touching the edge of the wire.

One advantage of skyrmions is their low susceptibility to external fields as uniform fields do not induce skyrmion displacement. The dynamics due to field gradients as discussed before is thus difficult to implement for devices. Furthermore, field-induced dynamics exhibits poor scaling when shrinking the size of a potential device. An alternative approach is current-induced magnetization manipulation, which exhibits favorable scaling.[5] Previously, current-induced magnetization dynamics due to spin-transfer torque effects has been in the focus of research. Here, the transfer of spin angular momentum from conduction electrons to the magnetization is used to efficiently manipulate magnetization in multilayer stacks with potential applications in magnetic random access memories[27] or to move domain walls,[5] which can be the basis for racetrack memory devices.[46]

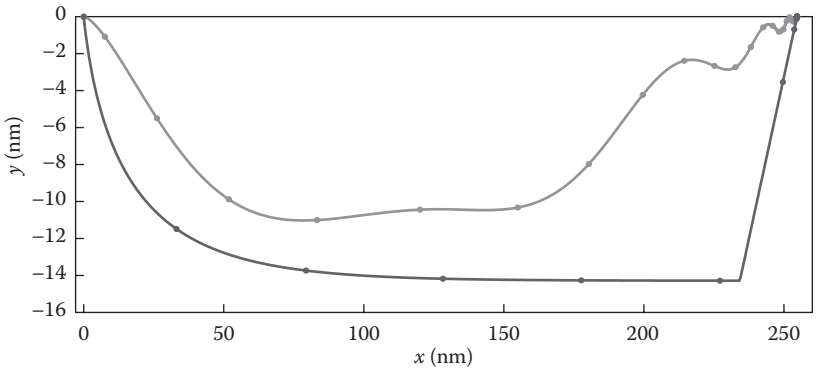

FIGURE 8.6 Trajectories of variable M skyrmions in wire geometry with a parabolic potential in y-direction. Light gray line: $M = 2 \times 10^{-21}$ kg. Dark gray line: $M = 0$. Both trajectories correspond to $G = 10^{-12}$ kg/s, $D\alpha = 7 \times 10^{-13}$ kg/s, and $K = 3.5 \times 10^{-3}$ N/m. The solid circles indicate time steps of 1 ns. (From Felix, B, *Nat. Phys.*, 11, 225–228, 2015. With permission.)

The adiabatic spin-transfer torque arises when an electron that traverses a spin structure continuously adjusts its spin orientation to match the local magnetization direction. For instance, if an electron passes adiabatically across a domain wall, it changes its spin direction by 180°. Due to conservation of angular momentum, a total of $1\hbar$ of angular momentum is transferred to the local spin structure in the process. Even when including nonadiabatic effects, the maximum angular momentum that an electron can transfer from its spin degree of freedom is $1\hbar$, and $1\hbar$/electron is hence a fundamental limit for the spin-transfer torque efficiency.

For the transfer of orbital angular momentum, however, there is no such fundamental limit and such a process can thus in principle be much more efficient. To transfer orbital angular momentum, one makes use of spin–orbit coupling in a heavy metal layer adjacent to a magnetic layer (Figure 8.8). Due to the SHE and the inverse spin galvanic effect (ISGE), the injected charge current j_{HM} leads to two torques acting on the magnetization. These two torques are distinct in their symmetry and are called field-like (FL) (sometimes also called reactive) and damping-like (DL) (sometimes also called dissipative or Slonczewski-like).[7] These torques result from two spin–orbit effects that occur in addition to spin-transfer torque:

1. When a charge current flows in a heavy metal layer, electrons experience a deflection that is perpendicular to their velocity and to their spin orientation. This so-called SHE leads to spin accumulations at all sides of the wire and each side has a different spin polarization, see Figure 8.7. Experimentally, a spin current flowing in z-direction (polarized in y-direction) is most interesting because it can be injected into a ferromagnet on top (or below) the HL, see Figure 8.8. The spin orientation in y-direction is called transverse polarization, to distinguish it from a longitudinal polarization (in the direction of current) and a perpendicular spin polarization (perpendicular to the interface). The transverse spin current that moves across the interface into the ferromagnet then interacts with the magnetization in the ferromagnetic layer via spin-transfer torque and thus manipulates the magnetization. Different microscopic origins have been proposed to explain this effect, including intrinsic band structure effects as well as extrinsic skew scattering and side jump effects.[60]
2. The ISGE (also termed Rashba–Edelstein effect) results from an electric field that originates from the symmetry breaking at the interface and then leads to an effective magnetic field for the

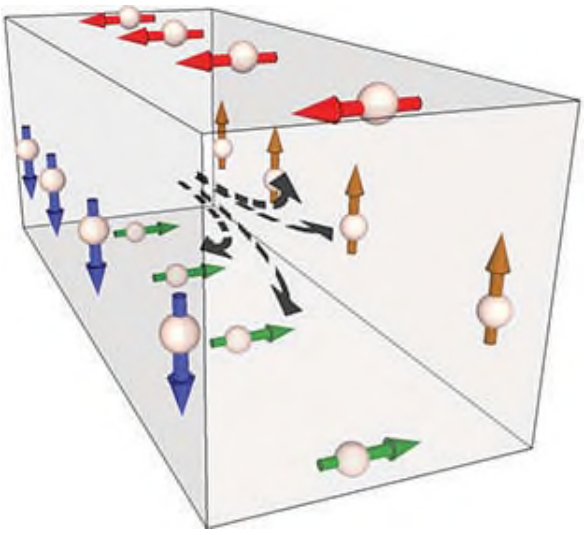

FIGURE 8.7 Illustration of the deflection of electrons in a heavy metal wire due to the spin Hall effect. Spheres indicate electrons and arrows their spin orientation. The dashed black arrows depict the electron trajectories. The electron flow is mostly along the wire axis, but due to the spin Hall effect, the electrons experience a deflection that depends on their spin orientation. In applications, typically a ferromagnetic layer would be placed on top or below the heavy metal layer and then experience an injection of spins that are polarized in a direction perpendicular to the current flow and perpendicular to the normal of the interface. (Reprinted from Pai, C.-F., *The spin Hall effect induced spin transfer torque in magnetic heterostructures*. PhD thesis, Cornell University, Ithaca, NY, 2015. With permission.)

moving electrons at the interface.[59] The sign of this field depends on the spin–orbit interaction and is independent of the Oersted field. It has a fixed direction at the interface within the sample, so that the spins moving at the interface experience a torque and a nonequilibrium spin density results. In contrast to the primarily bulk SHE, the ISGE is a pure interface effect only present in a multilayer configuration where the interface generates the required electric field. However, in such a multilayer configuration, the resulting spin density at the interface then acts by exchange on the magnetization in the ferromagnet and can thus manipulate it.

The damping-like torque and the field-like torque that can originate from the SHE or the ISGE are commonly called spin–orbit torques (SOTs). It is unclear and discussed controversially as to whether the ISGE alone can be responsible for the switching of the

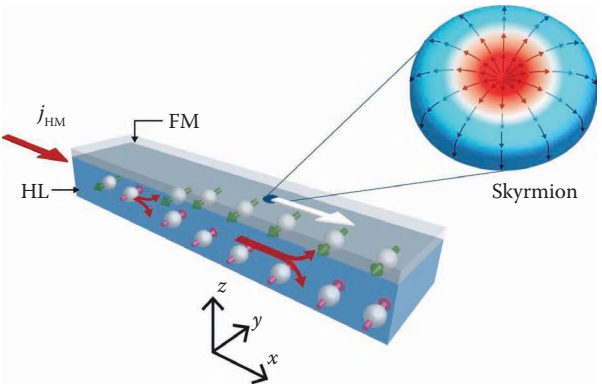

FIGURE 8.8 Schematic depiction of the multilayer stack suitable for spin–orbit torque-driven skyrmion motion. The multilayer consists of a heavy metal underlayer (HL) and a ferromagnetic layer (FL) where spin–orbit interaction effects, such as DMI and spin–orbit torques, occur. The injected charge current in the heavy metal layer j_{HM} along the x-direction in the HL splits due to the spin Hall effect, with spin-left electrons flowing up and spin-right electrons flowing down. Thus, a spin current in the z-direction with polarization in y-direction results. This spin current then acts on the magnetization in the FL. Furthermore, for electrons flowing at the interface, the inverse spin galvanic effect (sometimes also termed Rashba–Edelstein effect) leads to a nonequilibrium spin density and thus to an effective field at the interface that also acts on the magnetization in the FL. Both effects (spin Hall and inverse spin galvanic) lead to torques that can displace spin structures such as skyrmions (spin structure, see inset) along the wire with higher efficiency than the conventional approaches using spin-transfer torques.

perpendicular ferromagnetic layer, and the extent of the contribution from the SHE to the damping-like torque is not well known for metal systems. While originally it was predicted that the ISGE primarily leads to a field-like torque and the SHE to a damping-like torque, it is now generally accepted that both can lead to both torques.[21,33]

The current-driven motion of skyrmions in a thin transition metal ferromagnet at room temperature has recently been demonstrated experimentally.[70] In this experiment, Pt/Co/Ta and Pt/$Co_{60}Fe_{20}B_{20}$/MgO multilayer stacks with perpendicular magnetic anisotropy were studied with high-resolution magnetic transmission soft X-ray microscopy. Pt in contact with Co is known to generate strong DMI,[51] while Ta generates very weak DMI,[16] so that a large net DMI is anticipated in this asymmetric stack structure. Pt/$Co_{60}Fe_{20}B_{20}$/MgO multilayers are known for their low pinning due to the amorphous character of $Co_{60}Fe_{20}B_{20}$ and again the asymmetry in the stacking leads to a sizable DMI and SOT spin current.

Recent simulations suggest that skyrmions in ultrathin films might be driven even more efficiently than in previous studies of bulk materials due to the increased efficiency of vertical spin-current injection that is only available in thin film multilayers. Pt/FM/Ta multilayer stacks with a ferromagnet (FM) are very favorable in that regard because Pt and Ta have spin Hall angles of opposite signs, meaning that the spin current injected from Pt upwards has the same polarization as the spin current injected by Ta downwards. Hence, the spin Hall currents generated at each interface work in concert to generate a large damping-like torque.[71] As the spin Hall effect direction of motion of a skyrmion depends on the skyrmion topology, which in turn is here dominated by the DMI, observations of current-induced displacement can serve to unambiguously verify the topology and chirality of the skyrmions in this system.

In the experiment, an external magnetic field B_z was applied to a 2-μm wide magnetic track to shrink the zero-field labyrinth domains into a few isolated skyrmions. The track was contacted by Au electrodes at either end for current injection, as shown in Figure 8.9a. Figure 8.9b shows a sequence of images of a train of four skyrmions stabilized by B_z. Each image was acquired after injecting 20 current pulses with a current-density amplitude of 2.2×10^{11} A/m^2 and a duration of 20 ns. The pulse polarity is indicated in the figure. Three of the four skyrmions move freely along the track and can be displaced forward and backward by current, while the leftmost skyrmion (which is highlighted by a white circle) remains immobile, evidently pinned by a defect. The propagation direction is along the current flow direction (against electron flow), and this same directionality was observed for skyrmions with oppositely oriented cores. Micromagnetic simulations show that the observed unidirectional spin-Hall-driven displacement is consistent with Néel skyrmions with left-handed chirality, confirming the topological nature of the skyrmions in this material.[70]

The average skyrmion velocity was measured versus current density in three different devices, shown in Figure 8.9c. The experiment yields a critical current density of $j_{crit} = 2.0 \times 10^{11}$ A/m^2, below which skyrmions remain largely pinned. Slightly above j_{crit} the skyrmions move at different average speeds in different regions of the track, suggesting a significant influence of local disorder on the dynamics. Interestingly, pinned skyrmions can be annihilated, as seen in the last image of Figure 8.9b, where only three skyrmions remain, and the leftmost skyrmion becomes pinned at the same location as was

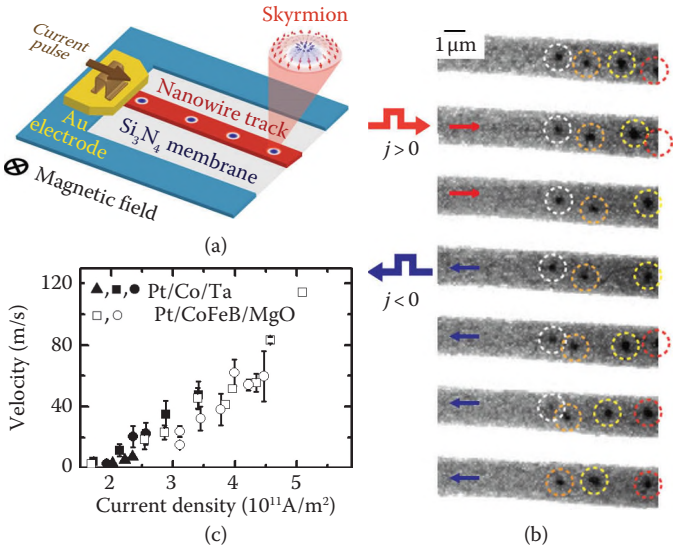

FIGURE 8.9 (a) Schematic of a magnetic track on Si_3N_4 membrane with current contacts and skyrmions stabilized by a down-directed applied magnetic field. (b) Sequential STXM images showing skyrmion displacement after injecting 20 unipolar current pulses along the track, with an amplitude and polarity as indicated. Individual skyrmions are outlined in dotted circles for clarity. (c) Average velocity of skyrmions in Pt/Co/Ta (closed symbols) and Pt/CoFeB/MgO (open symbols) versus current density; error bars denote standard deviation of multiple measurements. (From Woo, S. et al., *Nature Materials*, 15, 501–506, 2016. With permission.)

the annihilated skyrmion. At higher current densities, faster skyrmion motion with velocities exceeding 100 m/s has been detected.

The very large value of the experimentally observed critical current density and the skyrmion velocities that are lower than those calculated for a defect-free sample are in sharp contrast to recent micromagnetic studies that predict high skyrmion mobility even in the presence of discrete defects.[18,24,52] These micromagnetic simulations suggest that a dispersion in the anisotropy energy due to interface disorder has little influence on the dynamics. However, a short length scale dispersion in the local DMI can cause skyrmion pinning and thus leads to a finite critical current and reduced velocities, which is in qualitative agreement with our experiments. This suggests that even higher velocities and lower critical currents might be achieved by engineering materials and enhancing interface quality. However, even with the observed velocities, fast switching as necessary for devices can be achieved already.

These results show that magnetic skyrmions and skyrmion lattices can be stabilized in common polycrystalline transition metal ferromagnets and manipulated at high speeds in confined geometries at room temperature. Since the magnetic properties of thin-film heterostructures can be tuned over a wide range by varying layer thicknesses, composition, and interface materials, it is now possible to engineer the properties of skyrmions and their dynamics using materials that can be readily integrated into spintronic devices.

8.6 Experimental Challenges

Experimental investigations of magnetic skyrmions are difficult because of their small size: typically, the diameter of a skyrmion is less than 100 nm. Furthermore, confirming the skyrmion topology requires either an image of its 3D spin structure close to atomic resolution or a measurement of the behavior of the skyrmion with unambiguous signatures of the actual skyrmion topology, as illustrated for the example of the skyrmion trajectory in Figure 8.4. Images of the 3D magnetization can be reconstructed from Lorentz transmission electron microscopy (TEM) data, as first demonstrated by Yu et al.[72] (see Figure 8.10). The technique is very powerful for static or quasi-static measurements of skyrmions due to its high spatial resolution. Ultrafast dynamic imaging, however, is challenging

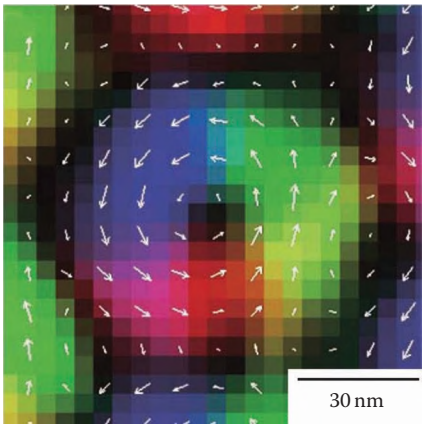

FIGURE 8.10 Real-space experimental image of a skyrmion. The image was acquired using Lorentz transmission electron microscopy. The color denotes the in-plane orientation of the magnetization, as indicated also by the arrows. Black areas are magnetized in the out-of-plane direction. (Reprinted by permission from Macmillan Publishers Ltd. [*Nature*] [Yu et al., 2010], copyright [2010]).

(1) because of the limited availability of stroboscopic TEM electron sources and (2) because the probing electrons of the TEM interact with the electric and magnetic fields that are normally used to excite dynamical behavior in magnetic systems. TEM pump-probe imaging of ferromagnetic domains has been available for decades, with nanometer spatial and sub-nanosecond temporal resolution.[4] However, thus far, no dynamic imaging of skyrmions using TEM has been reported.

Other ultra high spatial resolution imaging techniques with capabilities of detecting the spin configuration include scanning tunneling microscopy with a spin-polarized tip (SP-STM)[22] and nitrogen vacancy (NV) center magnetometry.[13,35] However, despite some advances in detecting spin waves with NV center magnetometry,[65,69] both techniques are presently not capable of pump-probe dynamic imaging.

There are several techniques suitable for pump-probe imaging of spin dynamics. The most common techniques are using light to probe the magnetic state, which is nonperturbative as long as heating of the sample is insignificant. Approaches using visible light, such as Kerr and Faraday microscopy, are widely accessible and have been successfully employed in studying bubble skyrmions for decades.[36] However, with some exceptions,[26] skyrmions in modern research are too small for visible light imaging. Therefore, X-ray imaging seems to be a rather appropriate method for imaging of skyrmion dynamics.

Generally, X-ray imaging techniques exploit the X-ray circular magnetic dichroism (XMCD)[56,63] to obtain X-ray absorption contrast for the spin component parallel to the propagation direction of the incident X-rays. A strong XMCD is observed when tuning the X-ray energy to the L-edge of the magnetic material, i.e., to wavelengths of a few nanometers. A weaker XMCD is found at the M-edge, i.e., at wavelengths of a few tens of nanometers. X-ray imaging techniques include transmission X-ray microscopy (TXM),[19] scanning transmission X-ray microscopy (STXM),[29] photo electron emission microscopy (PEEM),[32] and X-ray holography.[15] All of these techniques have been successfully employed in pump-probe imaging of spin dynamics and for imaging of skyrmions.[6,11,70]

Despite the many tools available for imaging of skyrmion dynamics, reports of such measurements are rare. The main challenge of such experiments is that pump-probe imaging requires one to repeat the experiment over and over again, and the dynamics of the specimen under investigation must be reproduced identically. Typically, a full movie with nanometer spatial and sub-nanosecond temporal

resolution requires billions of repetitions. Almost any magnetic material grown today, in particular, systems that host magnetic skyrmions show some irregularities in the magnetic potential landscape, so-called pinning. In such rough potentials, tiny deviations in the initial conditions or thermal effects can lead to large changes in the subsequent dynamics. Advances on reducing magnetic pinning have been reported,[10] and individual samples have indeed proven suitable for pump-probe imaging.[11] However, further advances are pivotal for systematic investigations of skyrmion dynamics and for their application in devices.

8.7 Outlook

In this chapter, we have discussed the topological identity of skyrmions and how they manifest in solid-state magnetism. We have provided the quasiparticle equation of motion of magnetic skyrmions and reviewed theoretical and experimental studies revealing their dynamics in the three important cases of (1) quasi-static motion, (2) gyrotropic relaxation, and (3) propagation in a wire. However, skyrmion research is a rapidly developing field with new results appearing all the time. Some of the new research directions that have recently emerged include new materials systems beyond the well-established B20 bulk inversion asymmetry compounds and the multilayer systems with structural inversion asymmetry as many other materials are fundamentally inversion asymmetric. These include GaV_4S_8,[28,50] Heusler compounds,[37] and nitrides (such as $CoRh_{0.75}Fe_{0.25}Mo_3N$), and others. Furthermore, while here we focus on the dynamics of skyrmions in ferromagnets, other materials' systems are starting to attract attention. This includes skyrmions in synthetic antiferromagnets[74] and skyrmions in antiferromagnetic single-layer systems.[1,73] In Figure 8.6, the trajectories of skyrmions can be seen for different effective masses for an effective force acting on the skyrmion. Clearly, in addition to the motion in the direction of the force, a perpendicular motion is observed. This is often termed an effective Magnus force.[49] A key advantage of using antiferromagnetic or antiferromagnetically coupled layers with skyrmions is the opposite action of the Magnus force on both sub-lattices (both layers) leading to no transverse motion for the skyrmion and thus a reduction in the interaction of a skyrmion for instance with a wire edge. Finally, novel manipulation of skyrmions beyond field (gradients) and currents include optical as well as electric-field excitations as some multiferroic systems exhibit DMI and host skyrmions.[58]

Acknowledgments

We gratefully acknowledge discussions and input from many previous and present collaborators, students, and colleagues. We thank Roberto Zivieri for checking and commenting on the equations that describe the skyrmion dynamics. For the micromagnetic simulations, we thank the Department of Physics of the University of Hamburg for access to the PHYSnet-Computing Center. Much of this work was funded by the German Ministry for Education and Science (BMBF) through the projects MULTIMAG (13N9911) and MPSCATT (05K10KTB), the EU's 7th Framework Programme MAGWIRE (FP7-ICT-2009-5 257707), the European Research Council through the Starting Independent Researcher Grant MASPIC (ERC-2007-StG 208162), the Mainz Center for Complex Materials (COMATT), the Center for Innovative and Emerging Materials (CINEMA), the Graduate School of Excellence Materials Science in Mainz (MAINZ GSC266), and the Deutsche Forschungsgemeinschaft (DFG).

References

1. J. Barker and O. A. Tretiakov. Static and Dynamical Properties of Antiferromagnetic Skyrmions in the Presence of Applied Current and Temperature, *Physical Review Letters*, 116: 147203, 2016.
2. A. A. Belavin and A. M. Polyakov. Metastable states of two-dimensional isotropic ferromagnets. *JETP Letters*, 22(10):245, 1975.
3. L. Berger. Exchange interaction between ferromagnetic domain wall and electric current in very thin metallic films. *Journal of Applied Physics*, 55(6):1954–1956, 1984.
4. O. Bostanjoglo and Th. Rosin. Resonance oscillations of magnetic domain walls and Bloch lines observed by stroboscopic electron microscopy. *Physica Status Solidi (a)*, 57(2):561–568, 1980.
5. O. Boulle, G. Malinowski, and M. Kläui. Current-induced domain wall motion in nanoscale ferromagnetic elements. *Materials Science and Engineering: R: Reports*, 72(9):159–187, 2011.
6. O. Boulle, et al. Room-temperature chiral magnetic skyrmions in ultrathin magnetic nanostructures. *Nature Nanotechnology*, 11(5):449–454, 2016.
7. A. Brataas and Kjetil M. D. Hals. Spin-orbit torques in action. *Nature Nanotechnology*, 9(2):86–88, 2014.
8. F. Büttner. *Topological mass of magnetic skyrmions probed by ultrafast dynamic imaging*. Dissertation, University of Mainz, Mainz, 2013.
9. F. Büttner, B. Krüger, S. Eisebitt, and M. Kläui. Accurate calculation of the transverse anisotropy of a magnetic domain wall in perpendicularly magnetized multilayers. *Physical Review B*, 92(5):054408, 2015.
10. F. Büttner, et al. Magnetic states in low-pinning high-anisotropy material nanostructures suitable for dynamic imaging. *Physical Review B*, 87(13):134422, 2013.
11. F. Büttner, et al. Dynamics and inertia of skyrmionic spin structures. *Nature Physics*, 11:225–228, 2015.

12. G. Chen, et al. Novel chiral magnetic domain wall structure in Fe/Ni/Cu(001) films. *Physical Review Letters*, 110(17):177204, 2013.
13. C. L. Degen. Scanning magnetic field microscope with a diamond single-spin sensor. *Applied Physics Letters,* 92(24):243111, 2008.
14. W. Döring. Über die Trägheit der Wände zwischen Weißchen Bezirken. *Z. Naturforsch. A*, 3:373, 1948.
15. S. Eisebitt, et al. Lensless imaging of magnetic nanostructures by X-ray spectroholography. *Nature*, 432(7019):885–888, 2004.
16. S. Emori, et al. Spin Hall torque magnetometry of Dzyaloshinskii domain walls. *Physical Review B*, 90(18):184427, 2014.
17. K. Everschor, M. Garst, R. A. Duine, and A. Rosch. Current-induced rotational torques in the skyrmion lattice phase of chiral magnets. *Physical Review B*, 84(6):064401, 2011.
18. A. Fert, V. Cros, and J. Sampaio. Skyrmions on the track. *Nature Nanotechnology*, 8(3):152–156, 2013.
19. P. Fischer, et al. Magnetic imaging with full-field soft X-ray microscopies. *Journal of Electron Spectroscopy and Related Phenomena*, 189:196–205, 2013.
20. J. H. Franken, M. Herps, H. J. M. Swagten, and B. Koopmans. Tunable chiral spin texture in magnetic domain-walls. *Scientific Reports*, 4:5248, 2014.
21. P. M. Haney, et al. Current induced torques and interfacial spin-orbit coupling: Semiclassical modeling. *Physical Review B*, 87(17):174411, 2013.
22. S. Heinze, et al. Spontaneous atomic-scale magnetic skyrmion lattice in two dimensions. *Nature Physics*, 7(9):713–718, 2011.
23. D. L. Huber. Equation of motion of a spin vortex in a two-dimensional planar magnet. *Journal of Applied Physics*, 53(3):1899–1900, 1982.
24. J. Iwasaki, M. Mochizuki, and N. Nagaosa. Current-induced skyrmion dynamics in constricted geometries. *Nature Nanotechnology*, 8(10):742–747, 2013.
25. J. Iwasaki, M. Mochizuki, and N. Nagaosa. Universal current-velocity relation of skyrmion motion in chiral magnets. *Nature Communications*, 4:1463, 2013.
26. W. Jiang, et al. Blowing magnetic skyrmion bubbles. *Science*, 349(6245):283–286, 2015.
27. A. D. Kent and D. C. Worledge. A new spin on magnetic memories. *Nature Nanotechnology*, 10(3):187–191, 2015.
28. I. Kézsmárki, et al. Neel-type skyrmion lattice with confined orientation in the polar magnetic semiconductor GaV_4S_8. *Nature Materials*, 14(11):1116–1122, 2015.
29. A. L. D. Kilcoyne, et al. Interferometer-controlled scanning transmission X-ray microscopes at the advanced light source. *Journal of Synchrotron Radiation*, 10(2):125–136, 2003.
30. N. S. Kiselev, A. N. Bogdanov, R. Schäfer, and U. K. Rößler. Comment on "giant skyrmions stabilized by dipole-dipole interactions in thin ferromagnetic films". *Physical Review Letters*, 107(17):179701, 2011.
31. W. Koshibae, et al. Memory functions of magnetic skyrmions. *Japanese Journal of Applied Physics*, 54(5):053001, 2015.
32. H. Kronmüller and S. Parkin, editors. *Handbook of Magnetism and Advanced Magnetic Materials, volume 3: Novel Techniques for Characterizing and Preparing Samples*. Wiley, 2007.
33. K. S. Lee, et al. Angular dependence of spin-orbit spin-transfer torques. *Physical Review B*, 91(14):144401, 2015.
34. I. Makhfudz, B. Krüger, and O. Tchernyshyov. Inertia and chiral edge modes of a skyrmion magnetic bubble. *Physical Review Letters*, 109(21):217201, 2012.

35. P. Maletinsky, et al. A robust scanning diamond sensor for nanoscale imaging with single nitrogen-vacancy centres. *Nature Nanotechnology*, 7(5):320–324, 2012.
36. A. P. Malozemoff and J. C. Slonczewski. *Magnetic Domain Walls in Bubble Materials*. Academic Press, New York, 1979.
37. O. Meshcheriakova, et al. Large noncollinearity and spin reorientation in the novel Mn_2RhSn Heusler magnet. *Physical Review Letters*, 113(8):087203, 2014.
38. T. Moriya. Anisotropic superexchange interaction and weak ferromagnetism. *Physical Review*, 120(1):91–98, 1960.
39. C. Moutafis, S. Komineas, and J. A. C. Bland. Dynamics and switching processes for magnetic bubbles in nanoelements. *Physical Review B*, 79(22):224429, 2009.
40. S. Mühlbauer, et al. Skyrmion lattice in a chiral magnet. *Science*, 323(5916):915–919, 2009.
41. J. Müller and A. Rosch. Capturing of a magnetic skyrmion with a hole. *Physical Review B*, 91(5):054410, 2015.
42. A. Neubauer, et al. Topological Hall effect in the A phase of MnSi. *Physical Review Letters*, 102(18):186602, 2009.
43. Y. Onose, et al. Observation of magnetic excitations of skyrmion crystal in a helimagnetic insulator Cu_2OSeO_3. *Physical Review Letters*, 109(3):037603, 2012.
44. C. F. Pai. *The spin Hall effect induced spin transfer torque in magnetic heterostructures*. PhD thesis, Cornell University, Ithaca, NY, 2015.
45. N. Papanicolaou and T.N. Tomaras. Dynamics of magnetic vortices. *Nuclear Physics B*, 360(2–3):425–462, 1991.
46. Stuart S. P Parkin, M. Hayashi, and L. Thomas. Magnetic domain-wall racetrack memory. *Science*, 320(5873):190–194, 2008.
47. S. Rohart and A. Thiaville. Skyrmion confinement in ultrathin film nanostructures in the presence of Dzyaloshinskii-Moriya interaction. *Physical Review B*, 88(18):184422, 2013.
48. N. Romming, et al. Writing and deleting single magnetic skyrmions. *Science*, 341(6146):636–639, 2013.
49. A. Rosch. Skyrmions: Moving with the current. *Nature Nanotechnology*, 8(3):160–161, 2013.
50. E. Ruff, et al. Multiferroicity and skyrmions carrying electric polarization in GaV_4S_8. *Science Advances*, 1(10):e1500916, 2015.
51. K. S. Ryu, L. Thomas, S. H. Yang, and S. Parkin. Chiral spin torque at magnetic domain walls. *Nature Nanotechnology*, 8(7):527–533, 2013.
52. J. Sampaio, et al. Nucleation, stability and current-induced motion of isolated magnetic skyrmions in nanostructures. *Nature Nanotechnology*, 8:839–844, 2013.
53. T. Schulz, et al. Emergent electrodynamics of skyrmions in a chiral magnet. *Nature Physics*, 8(4):301–304, 2012.
54. C. Schütte and M. Garst. Magnon-skyrmion scattering in chiral magnets. *Physical Review B*, 90(9):094423, 2014.
55. C. Schütte, J. Iwasaki, A. Rosch, and N. Nagaosa. Inertia, diffusion, and dynamics of a driven skyrmion. *Physical Review B*, 90(17):174434, 2014.
56. G. Schütz, et al. Absorption of circularly polarized x rays in iron. *Physical Review Letters*, 58(7):737–740, 1987.
57. T. Schwarze, et al. Universal helimagnon and skyrmion excitations in metallic, semiconducting and insulating chiral magnets. *Nature Materials*, 14(5):478–483, 2015.
58. S. Seki, X. Z. Yu, S. Ishiwata, and Y. Tokura. Observation of skyrmions in a multiferroic material. *Science*, 336(6078):198–201, 2012.

59. Ka Shen, G. Vignale, and R. Raimondi. Microscopic Theory of the inverse Edelstein effect. *Physical Review Letters*, 112(9):096601, 2014.
60. J. Sinova, et al. Spin Hall effects. *Reviews of Modern Physics*, 87(4):1213–1260, 2015.
61. T.H.R. Skyrme. A unified field theory of mesons and baryons. *Nuclear Physics*, 31:556–569, 1962.
62. J.C. Slonczewski. Current-driven excitation of magnetic multilayers. *Journal of Magnetism and Magnetic Materials*, 159(1–2):L1–L7, 1996.
63. J. Stöhr and H. C. Siegmann. *Magnetism - From Fundamentals to Nanoscale Dynamics*. Springer-Verlag, Berlin, Heidelberg, 2006.
64. O. Tchernyshyov and G. W. Chern. Fractional vortices and composite domain walls in flat nanomagnets. *Physical Review Letters*, 95(19):197204, 2005.
65. J.-P. Tetienne, et al. Nanoscale imaging and control of domain-wall hopping with a nitrogen-vacancy center microscope. *Science*, 344(6190):1366–1369, 2014.
66. A. Thiaville, Y. Nakatani, J. Miltat, and Y. Suzuki. Micromagnetic understanding of current-driven domain wall motion in patterned nanowires. *EPL (Europhysics Letters)*, 69(6):990, 2005.
67. A. A. Thiele. Steady-state motion of magnetic domains. *Physical Review Letters*, 30(6):230–233, 1973.
68. R. Tomasello, et al. A strategy for the design of skyrmion racetrack memories. *Scientific Reports*, 4:6784, 2014.
69. T. van der Sar, F. Casola, R. Walsworth, and A. Yacoby. Nanometre-scale probing of spin waves using single electron spins. *Nature Communications*, 6:7886, 2015.
70. S. Woo, et al. Observation of room-temperature magnetic skyrmions and their current-driven dynamics in ultrathin metallic ferromagnets. *Nature Materials*, 15:501–506, 2016.
71. S. Woo, et al. Enhanced spin-orbit torques in Pt/Co/Ta heterostructures. *Applied Physics Letters*, 105(21):212404, 2014.
72. X. Z. Yu, et al. Real-space observation of a two-dimensional skyrmion crystal. *Nature*, 465(7300):901–904, 2010.
73. X. Zhang, Y. Zhou, and M. Ezawa. Antiferromagnetic skyrmion: Stability, creation and manipulation. *Scientific Reports*, 6:24795, 2016.
74. X. Zhang, Y. Zhou, and M. Ezawa. Magnetic bilayer-skyrmions without skyrmion Hall effect. *Nature Communications*, 7:10293, 2016.
75. Y. Zhou, et al. Dynamically stabilized magnetic skyrmions. *Nature Communications*, 6:8193, 2015.
76. Y. Zhou and M. Ezawa. A reversible conversion between a skyrmion and a domain-wall pair in a junction geometry. *Nature Communications*, 5:4652, 2014.